とぴっくす

Structural investigation of radiation-grafted polymer electrolyte membrane by SANS partial scattering function analysis

国立研究開発法人 量子科学技術研究開発機構
趙 躍*, 吉村 公男, 廣木 章博, 前川 康成

Radiation-grafted polymer electrolyte membranes (PEMs) are a promising alternative to the benchmark material Nafion® used for electrochemical devices like electrodialysis and fuel cells. To facilitate their applications, thorough understanding of the structure of this type PEMs is crucial. In this report, we introduced the partial scattering function (PSF) analysis through the contrast variation small-angle neutron scattering technique to quantitatively elucidate the hierarchical structure of the radiation-grafted PEM, made of poly(styrene sulfonic acid) grafting onto poly(ethylene-co-tetrafluoroethylene) base films, from micro- /nano- meter scale to molecular level. The analysis on PSF self-terms gave the exact structure of individual components and that on cross-terms explored the correlation between two components to establish their locations. The results provided mechanistic insights into membrane conductivity and structure correlations.

Keywords: contrast variation small-angle neutron scattering, partial scattering function, radiation-grafted polymer electrolyte membrane

1 Introduction

Radiation-induced grafting polymerization is used in the manufacture of many products, such as diaphragms for button batteries and ion exchange membranes for salt production. Recently, this technique has been used to fabricate polymer electrolyte membranes (PEMs) for applications in fuel cells and other electrochemical devices. It allows for imparting new functionalities by graft polymers containing ionic groups and maintaining the excellent mechanical/thermal properties of the base polymer. Among extensively studied base polymers, partially fluorinated poly(ethylene-co-tetrafluoroethylene) (ETFE) has been identified as a good candidate due to its outstanding thermal/mechanical properties and high resistance to radiation. The fabrication of ETFE-based PEM includes radiation-induced grafting monomers onto ETFE base films followed by ionization[1,2]. The resultant PEMs such as poly(styrenesulfonic acid)-grafted ETFE (ETFE-g-PSSA) were found to have initially comparable fuel cell performance to the benchmark material, Nafion®[2]. However, challenges still remain for ETFE-g-PSSA PEMs such as the low proton conductivity under reduced relative humidity and long-term stability. To overcome these obstacles, we have to understand the structure-property relationships of the membrane[1–3].

It is well known that in a hydrated ETFE-g-PSSA PEM, the sulfonic acid groups on the graft polymer absorb water and form ion-conducting nano-channels through which protons migrate and the conductivity is generated. These hydrophilic channels are embedded in but microphase segregated from the hydrophobic base polymer matrix. The morphology, size and connectivity of hydrophilic channels and hydrophobic base polymer domains severely influence PEM conductivity and stability, respectively. To elucidate these structures, the scattering techniques such as small-angle X-ray scattering (SAXS) and small-angle neutron scattering (SANS) are regarded as a powerful tool due to the high space resolution covering wide length scales from micro-/nano- meter down to molecular level. Note that the scattering power of the element is proportional to its electron density for X-ray, while for neutrons it varies irregu-

Structural investigation of radiation-grafted polymer electrolyte membrane by SANS partial scattering function analysis
Yue Zhao*, Kimio Yoshimura, Hiroki Akihiro and Yasunari Maekawa (*National Institutes for Quantum Science and Technology*),
〒370–1292 群馬県高崎市綿貫町 1233
TEL: 027–346–9100, FAX: 027–346–9385,
E-mail: zhao.yue@qst.go.jp

larly with the atomic number. As a result, neutrons might be more efficient to explore water channels in the hydrated PEMs than X-ray[4–8]. In conventional scattering analysis, a scattering intensity profile, $I(q)$, is plotted as a function of the scattering vector, q. The typical SANS $I(q)$ profile of ETFE-g-PSSA PEMs usually shows two scattering characteristics: a broad peak in the low-q range at $0.1 < q < 0.3$ nm^{-1}, corresponding to the microphase separation between graft polymer domains and base polymer matrix due to their immiscibility; and a second peak in the high-q range at $1.5 < q < 3$ nm^{-1}, so-called the "ionomer peak", associating with hydrophilic water domains and channels. To analyze $I(q)$, the proper structure model is usually presumed to describe the typical structure pattern of a system without assigning components. Since the $I(q)$ profile contains the scattering contributions from all the components, i.e., hydrophobic polymer, hydrophilic polymer, and water, one may neither separately identify the structure of each component nor offer the location assignment. To solve this problem, we recently developed partial scattering function (PSF) analysis by the quantitative decomposition of intensity profiles through contrast-variation SANS (CV-SANS) method[4–6]. This benefits from the unique possibility of neutron scattering that uses isotope labeling with deuterium, i.e., the coherent scattering length of the hydrogen (−3.74 fm) is much different from deuterium (6.67 fm). Therefore, contrast variation can be performed based on the hydrogen/deuterium replacement with neutrons as a probe.

In this article, we introduce the PSF analysis through CV-SANS to determine the detailed structure of ETFE-g-PSSA PEMs. The unique capability that PSF analysis provides to understanding structure correlations can result into new insights on the role of the polymer micro-/nanostructure and water in the emergence of the ion conduction.

2 Theoretical decomposition of scattering intensities into PSFs by CV-SANS

We consider a general PEM composed of three components 1, 2, and 3, being the hydrophobic polymer, the hydrophilic polymer with ionic groups, and absorbed water, respectively. Thus, $I(q)$ can be split into three PSF self-terms, S_{ii}, based on the incompressibility hypothesis,

$$\begin{aligned} I(q) = {} & (b_1 - b_2)(b_1 - b_3)S_{11}(q) \\ & + (b_2 - b_1)(b_2 - b_3)S_{22}(q) \\ & + (b_3 - b_1)(b_3 - b_2)S_{33}(q) \end{aligned} \tag{1}$$

where b_i is the scattering length density (SLD) of the i component. S_{ii} is defined as,

$$S_{ii}(q) = \frac{1}{V}\left\{\iint \delta\varphi_i(\vec{\mathrm{r}})\,\delta\varphi_i(\vec{\mathrm{r}'})\exp\left[-i\vec{q}\left(\vec{\mathrm{r}}-\vec{\mathrm{r}'}\right)\right]d\vec{\mathrm{r}}\,d\vec{\mathrm{r}'}\right\} \tag{2}$$

where V is the scattering volume and $\delta\phi_i(\vec{\mathrm{r}})$ is the fluctuation of the volume fraction of the i component at position $\vec{\mathrm{r}}$. S_{ii} is the Fourier transform of the autocorrelation function of $\delta\phi_i(\vec{\mathrm{r}})$ and therefore gives the structural information.

CV-SANS experiments are performed with m different contrasts by using H_2O/D_2O mixtures, the obtained $I(q)$s are a group of linear equations of Eq. (1), expressed as below,

$$\begin{pmatrix} I_1(q) \\ \vdots \\ I_m(q) \end{pmatrix} = \boldsymbol{M} \cdot \begin{pmatrix} S_{11}(q) \\ S_{22}(q) \\ S_{33}(q) \end{pmatrix} \tag{3}$$

where $\boldsymbol{M}$ is the coefficient matrix as expressed below,

$$\boldsymbol{M} = \begin{pmatrix} {}^1\Delta_{12}\,{}^1\Delta_{13} & {}^1\Delta_{21}\,{}^1\Delta_{23} & {}^1\Delta_{31}\,{}^1\Delta_{32} \\ \vdots & \vdots & \vdots \\ {}^m\Delta_{12}\,{}^m\Delta_{13} & {}^m\Delta_{21}\,{}^m\Delta_{23} & {}^m\Delta_{31}\,{}^m\Delta_{32} \end{pmatrix} \tag{4}$$

where ${}^m\Delta_{ij} = {}^m(b_i - b_j)$ is the SLD difference between i and j in m-th measurement. Note that the change in the SLD of polymers in CV-SANS experiments is negligible, therefore, b_1 and b_2 are constants, which can be theoretically calculated by their chemical structure and mass density.[7] On the contrary, b_3 for water component varies as a function of volume fraction of D_2O (f_{D_2O}) in water mixtures given below,

$$b_3 = b_{D_2O} f_{D_2O} + b_{H_2O}(1 - f_{D_2O}) \tag{5}$$

with b_{D_2O} and b_{H_2O} being the SLD of D_2O and H_2O being 6.34 and −0.56 ($\times 10^{10}$ cm^{-2}), respectively. Thus $S_{11}(q)$, $S_{22}(q)$ and $S_{33}(q)$ on the right side of Eq. (3) can be mathematically determined through the series of $I(q)$[4–6]. The PSF cross-term $S_{ij}(i \neq j)$ can be expressed by S_{ii} using relationships of $S_{12} = \frac{1}{2}(S_{33} - S_{11} - S_{22})$, $S_{23} = \frac{1}{2}(S_{11} - S_{22} - S_{33})$, $S_{13} = \frac{1}{2}(S_{22} - S_{11} - S_{33})$.

S_{ii} reflects the structure of the i component, and is always positive. Whereas S_{ij} indicates the interaction be-

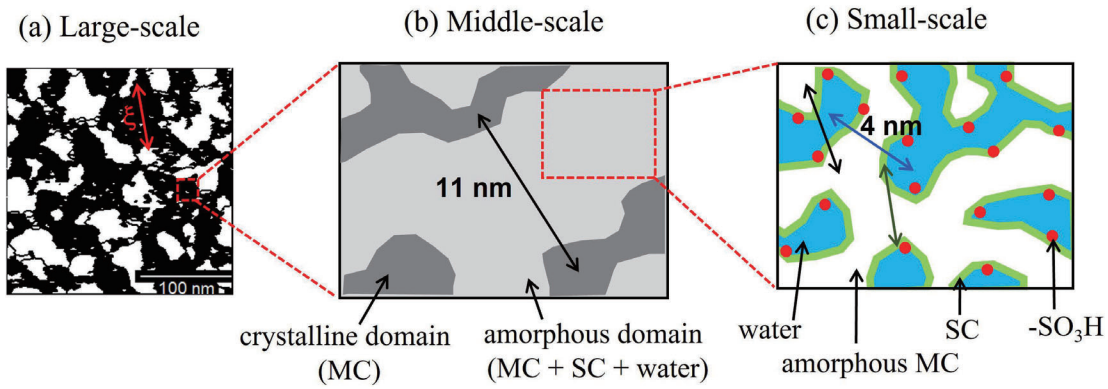

Figure 1. Schematic of the hierarchical structure of individual components in the fully hydrated Nafion membrane. Reprinted with permission from Macromolecules 2021, 54, 4128–4135. Copyright [2021] American Chemical Society.

tween the i and j components, i.e., the positive and negative signs mean attractive and repulsive interactions, respectively. Therefore, S_{ij} may give the relative positions of the i and j components.

3 PSF analysis on PEMs

To certify the validity of PSF analysis on PEMs, we first applied it to elucidate the structure of the benchmark PEM, Nafion® (NR-212, DuPont). The hydrated Nafion membrane is composed of hydrophobic tetrafluoroethylene-like main-chain (MC), the hydrophilic perfluoroalkyl ether sulfonic acid side-chain (SC), and water, in accordance with components 1–3 defined in section 2, respectively. Using the abovementioned decomposition method, both S_{ii} and S_{ij} were calculated through CV-SANS results as detailed in Ref. 5). The structure determination was based on the best-fitting of structure models to S_{ii}, including the Debye-Bueche (DB) model describing the structure heterogeneity in small-q region, and the Teubner-Strey (TS) model describing bicontinuous-shaped morphology in the middle- and high-q regions. The analysis on S_{ij} showed interactions between MC and SC, and between SC and water are repulsive, but that between SC and water is always attractive.

PSF analysis allowed us, for the first time, to visualize the structure pattern of individual components in Nafion as illustrated in Fig. 1. In the large scale, structural heterogeneity with a size of > 65 nm was found in the MC and SC domains but not in water domains. In the middle scale, bicontinuous-like structure of crystalline and amorphous phases with a mean separation distance of 11 nm was observed. In the small scale, bicontinuous-like structure of SC domains and water domains existed in the amorphous phase with a mean separation distance of about 4 nm.

The successful demonstration of Nafion structure substantially increased the impact of the PSF analysis. Following the strategy, we applied the analysis to radiation grafted ETFE-g-PSSA PEM with an ion exchange capacity (IEC) of 2.0 mmol/g[6]. The components 1–3 represent ETFE base polymer (BP, -$CH_2CH_2CF_2CF_2$-), PSSA graft polymer (GP, -C_8H_7-SO_3H), and water, respectively. CV-SANS measurements were performed on KWS-2 SANS diffractometer operated by Juelich Centre for Neutron Science at the neutron source Heinz Maier-Leibnitz (FRM II reactor), and the fully hydrated ETFE-g-PSSA PEMs were prepared in H_2O/D_2O mixtures with different f_{D_2O} ranging from 0 to 100 %[8]. $I(q)$ profiles at representative f_{D_2O} are shown in Fig. 2. Superior to the conventional SANS measurement in that only a single profile usually being measured, i.e., $I(q)$ at f_{D_2O} = 100 % shown in Fig. 2, unable to distinguish a system composed of two or more components, CV-SANS clearly provides a measure. According to Babinet's principle, if the system is made of two components, contrast variation will change the absolute intensity but not the shape of the scattering profiles[7]. Figure 2 confirmed that the hydrated ETFE-g-PSSA PEM is not a "two-component" system, and hence it is better to be described by the three-component model proposed in Section

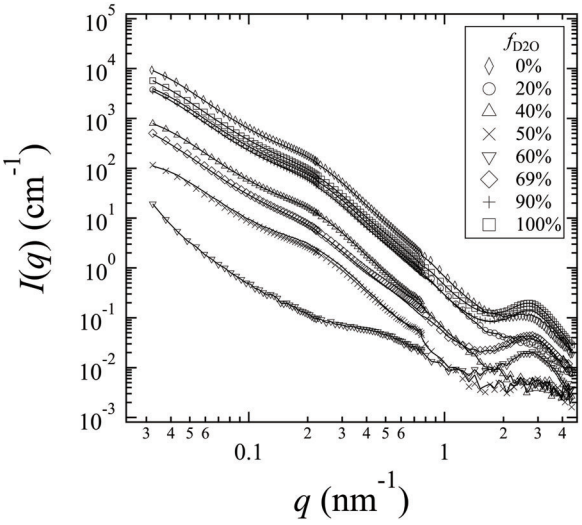

Figure 2. CV-SANS $I(q)$ profiles of fully hydrated ETFE-g-PSSA PEMs at representative f_{D_2O}. Adapted with permission from Macromolecules 2022, 55, 7100–7109. Copyright [2022] American Chemical Society.

2. The decomposition of CV-SANS data gave S_{ii} and S_{ij}, which were plotted in Figs. 3(a) and 3(b), respectively.

S_{ii} in Figure 3(a) shows a clear upturn with a power-law exponent of −2.4 in Region I ($q < 0.12$ nm^{-1}), a shoulder-like scattering maximum with a center position at q_1 = 0.2 nm^{-1} in Region II ($0.12 < q < 1.5$ nm^{-1}), and a peak with a center position at q_2 = 2.7 nm^{-1} for S_{22} and S_{33} in Region III ($q > 1.5$ nm^{-1}). Note that S_{11} in Region III is flat, revealing BP is structureless at this length scale.

To interpret structures, several structural models were proposed to fit S_{ii}. In Region I, the mass fractal (MF) structure model, $S_{MF}(q) \sim q^{-D_f}$, with D_f being the fractal dimension, was used to describe densely packed GP nanodomains in the BP matrix. This is based on the microphase separation between BP and GP during the graft polymerization resulting in the aggregation of individual GP domains. In Region II, Guinier-exponential (GE) function,

$$S_{GE}(p) \sim \exp\left(\frac{-q^2R_g^2}{3}\right) + B\left\{\frac{\left[\mathrm{erf}\left(\frac{kqR_g}{\sqrt{6}}\right)\right]^3}{q}\right\}^P \quad ,$$

was used to describe the irregular shaped individual GP domains, where R_g is the particle's radius of gyration, erf

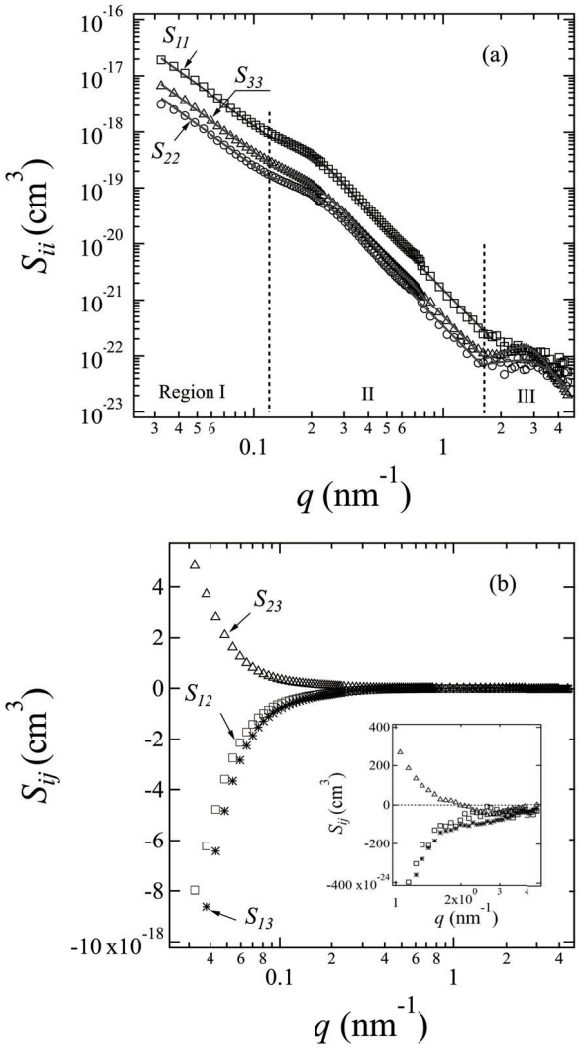

Figure 3. (a) S_{ii} of the fully hydrated ETFE-g-PSSA PEMs (symbols) and the best-fitted results (solid lines). (b) S_{ij} of the fully hydrated ETFE-g-PSSA PEMs. Enlarged plot in the inset. Adapted with permission from Macromolecules 2022, 55, 7100–7109. Copyright [2022] American Chemical Society.

is the error function, k is an empirical constant of 1.06, and $P(3 < P < 4)$ is the particle's surface fractal dimension, and B is a constant prefactor. In Region III, TS model,

$$S_{TS}(q) \sim \frac{8\pi d^4}{\varepsilon[16\pi^4 + 8d^2\pi^2(\varepsilon^{-2} + q^2)^2]} \quad ,$$

was used to fit S_{22} and S_{33}, describing bicontinuous-shaped local morphology of the GP and water domains, with d and ε being the mean distance between two

Table 1. Best-fitting parameters by MF, GE, and TS structural models. Adapted with permission from Macromolecules 2022, 55, 7100–7109. Copyright [2022] American Chemical Society.

Models	MF Model	GE Model		TS Model	
S_{ii}	D_f	R_g(nm)	P	d (nm)	ε (nm)
S_{11}	2.4 ± 0.1	9.5 ± 0.2	3.50 ± 0.05	-	-
S_{22}	2.4 ± 0.1	9.5 ± 0.2	3.50 ± 0.05	1.9 ± 0.1	0.47 ± 0.02
S_{33}	2.4 ± 0.1	9.5 ± 0.2	3.50 ± 0.05	2.0 ± 0.1	0.58 ± 0.02

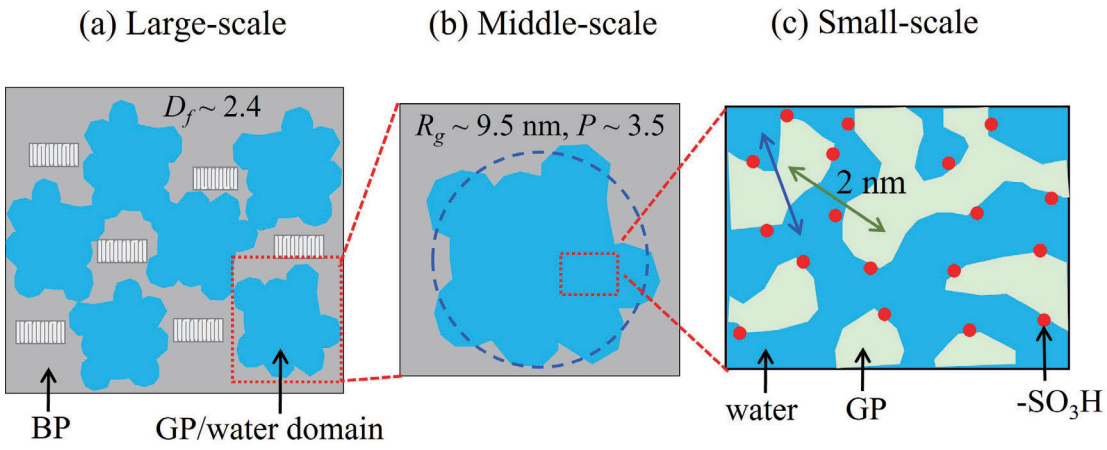

Figure 4. Schematic of the hierarchical structure of individual components in the fully hydrated ETFE-g-PSSA PEMs. Adapted with permission from Macromolecules 2022, 55, 7100–7109. Copyright [2022] American Chemical Society.

domains and the dispersion of d, respectively. These structural models provided adequate fits to the data as shown in solid lines in Fig. 3(a). The detailed structure evolution can be found in Ref. 6), and the fitting parameters are listed in Table 1.

Figure 3(b) shows that S_{12} and S_{13} are negative, suggesting that BP domains tend to phase-separate from either GP or water domains. Therefore, the incorporation of GP domains in the BP matrix adds its structural pattern to the original BP matrix. It explained why S_{11} showed the same MF structure and GE structure features as S_{22}. On the other hand, S_{23} is found to be positive at $q < 2$ nm^{-1}, indicating the attraction between GP and water, and hence GP and water domains must be closely attached through sulfonic acid groups and move coordinately at the length scale > 3 nm. Thus, water domains form aggregates in the same way as GP domains, giving the same MF structure and GE structure as GP. It was surprising to find that S_{23} becomes negative at $q > 2$ nm^{-1} in Region III, suggesting a repulsion between GP and water at the molecular length level < 3 nm. This result is rather different from Nafion where an attractive interaction between side-chain and water exists from microscopic scale to molecular levels. This structure difference results in a much higher hydration number (number of water molecules per SO_3H) for Nafion being ~23 than that for ETFE-g-PSSA PEMs being ~11 under the same hydrated condition. It is believed to be the main reason for the low swelling but high conductivity of ETFE-g-PSSA PEM under fully hydrated conditions.

We summarized the results and constructed the entire structure pattern of ETFE-g-PSSA PEMs in Fig. 4. In the large scale, aggregates of GP/water domains in a mass fractal structure with a fractal dimension of 2.4 were formed and well phase-separated with the ETFE BP matrix. In the middle scale, the individual GP/water domain made of homogeneously incorporated GP and water with

an average size of R_g = 9.5 nm was observed. In the small scale, both GP and water showed a bicontinuous-like local structure, indicating the formation of a well-connected ion channel network, a key structural factor for the high membrane conductivity that was claimed in Nafion membranes.

4 Conclusion and future perspectives

We developed PSF analysis through CV-SANS experiments to gain quantitative knowledge of the role of each component in the entire structure of fully hydrated PEMs. The method was successfully verified in the benchmark material Nafion, and then applied to the radiation-grafted ETFE-g-PSSA PEMs. PSF self-terms analysis revealed the detailed structure of individual components, whereas the cross-terms gave the interactions among components. PSF analysis provides mechanistic insights concerning multiple length scale structural correlations. In particular, the structural guidelines at the molecular level in turn can help in the design of high-performing PEMs for a wide range of energy conversion applications.

〈参 考 文 献〉

1) M. M. Nasef, Chem. Rev., 114 (2014) 12278.
2) J. A. Horsfall, K. V. Lovell, Fuel Cells, 1 (2001) 186.
3) S. A. Gürsel, L. Gubler, B. Gupta, G. G. Scherer, Fuel Cells I, Springer, Berlin, 2008.
4) H. Endo, D. Schwahn, H. Colfen, J. Chem. Phys., 120 (2004) 9410.
5) Y. Zhao, K. Yoshimura, T. Motegi, A. Hiroki, A. Radulescu, Y. Maekawa, Macromolecules, 54 (2021) 4128.
6) Y. Zhao, K. Yoshimura, S. Sawada, T. Motegi, A. Hiroki, A. Radulescu, Y. Maekawa, Macromolecules, 55 (2022) 7100.
7) R. J. Roe, Methods of X-ray and neutron scattering in polymer science, Oxford University Press, New York, 2000.
8) A. Radulescu, V. Pipich, H. Frielinghaus, M. S. Appavou, J. Phys.: Conf. Ser., 351 (2012) 012026.

〈著 者 略 歴〉

趙 躍： 2003 年中国科学技術大学化学材料科学学院化学物理系博士課程修了，2010 年日本原子力研究開発機構（現 量子科学技術研究開発機構）入社，ナノ構造制御高分子材料プロジェクトリーダー（現職）．専門：高分子物理化学，小角散乱技術．

吉村 公男： 2009 年群馬大学大学院ナノ材料システム工学専攻博士後期課程修了，2016 年量子科学技術研究開発機構入社，主幹研究員．専門：有機合成化学，高分子機能材料．

廣木 章博： 2001 年群馬大学大学院工学研究科物質工学専攻博士後期課程修了，2006 年日本原子力研究開発機構（現 量子科学技術研究開発機構）入社，主幹研究員．専門：放射線化学，高分子機能材料．

前川 康成： 1991 年東京大学大学院工学系研究科合成化学専攻博士課程修了，1998 年日本原子力研究所（現 量子科学技術研究開発機構）入所，2005 年グループリーダー，2022 年所長（現職）．専門：放射線化学，高分子機能材料．